

Intrazeolitic Photochemical Charge Separation for $\text{Ru}(\text{bpy})_3^{2+}$ –Bipyridinium System: Role of the Zeolite Structure

Marcello Vitale, Norma B. Castagnola, Nancy J. Ortins, James A. Brooke, Anand Vaidyalingam, and Prabir K. Dutta*

Department of Chemistry, The Ohio State University, 100 West 18th Avenue, Columbus, Ohio 43210

Received: September 1, 1998; In Final Form: February 10, 1999

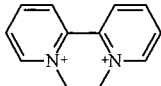
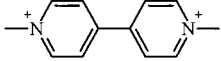
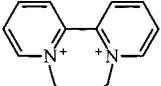
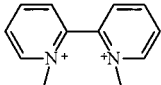
The pore structure of zeolite Y consists of 13 Å supercages connected through 7 Å windows. This study deals with the intrazeolitic photoelectron transfer from trisbipyridyl ruthenium (II) ($\text{Ru}(\text{bpy})_3^{2+}$) synthesized within zeolite Y supercages to ion-exchanged bipyridinium molecules in neighboring supercages. Three *N,N'*-dialkyl-2,2'-bipyridinium ions and a 4,4'-bipyridinium ion with reduction potentials varying from -0.37 to -0.65 V have been studied. For the 2,2'-bipyridinium salts (members of the diquat family), two, three, and four CH_2 bridging units abbreviated as 2DQ^{2+} , 3DQ^{2+} , and 4DQ^{2+} , respectively, have been examined. The fourth viologen is 1,1'-dimethyl-4,4'-bipyridinium, commonly known as methyl viologen and abbreviated here as MV^{2+} . Because of the limitations of the time-resolved diffuse reflectance instrument, only a lower limit of the forward electron transfer rate constant from $\text{Ru}(\text{bpy})_3^{2+}$ to the bipyridinium ion was obtained and is $>10^7 \text{ s}^{-1}$. The back electron transfer from the photogenerated bipyridinium radical ions to $\text{Ru}(\text{bpy})_3^{3+}$ was monitored at different intrazeolitic bipyridinium concentrations. At low loadings of bipyridinium ions (1 per 10–15 supercages), the transient signal between 360 and 390 nm has contributions from both $\text{Ru}(\text{bpy})_3^{2+}$ and the bipyridinium radical ions, since the bipyridinium ion concentration was not high enough to quench all of the $\text{Ru}(\text{bpy})_3^{2+}$. The decay of this signal (360–390 nm) could be fitted to the sum of two exponentials, representing the disappearance of unquenched $\text{Ru}(\text{bpy})_3^{2+}$ and the back electron transfer from the bipyridinium radical ions to $\text{Ru}(\text{bpy})_3^{3+}$. The rate constants for the back electron transfer for 2DQ^{2+} , MV^{2+} , 3DQ^{2+} , and 4DQ^{2+} were found to be 4.0×10^4 , 1.7×10^4 , 1.1×10^4 , and $7.3 \times 10^3 \text{ s}^{-1}$. The decrease in the electron transfer rates with increasing driving force for the reaction indicates that the electron transfer is occurring in the Marcus inverted region. At high loadings of the bipyridinium ions (1.2–1.7 molecules/supercage), the bipyridinium radical ions were considerably longer lived, and a simple exponential decay no longer described the loss of the bipyridinium radical signal. A model that allows for electron exchange processes between bipyridinium ions to compete with the back electron transfer was necessary. This kinetic model allowed us to extract the back electron transfer rate at high loadings along with the rate constants for electron hopping and a second-order electron (bipyridinium radical)/hole ($\text{Ru}(\text{bpy})_3^{3+}$) recombination process. For the series 2DQ^{2+} , MV^{2+} , 3DQ^{2+} , and 4DQ^{2+} with high loading, the back electron transfer rate constants were 2.5×10^5 , 9×10^4 , 1.8×10^5 , and $1.2 \times 10^5 \text{ s}^{-1}$, higher than the low loading samples. In the high loading case, longer lived charge separation was observed because of the presence of a route for charge propagation by electron hopping via the densely packed viologen molecules.

Practical solar energy conversion processes, such as the production of useful chemicals (e.g., H_2 and O_2) from plentiful sources (e.g., water) is an active area of research.¹ A fundamental issue that limits the development of solar energy conversion is the thermal back electron transfer between the photochemically generated redox pairs prior to the accomplishment of any useful chemistry.² Considerable effort is being spent in developing molecular assemblies that lead to long-lived charge separation.³ Another approach is to use microheterogeneous supports in aiding the charge separation process.⁴ Aluminosilicate zeolites have shown considerable promise for promoting stabilization of photochemically generated redox species.⁵ The arrangement of cages and channels in these crystalline zeolites allows for placement of molecules in well-defined and unique spatial arrangements. Trisbipyridine ruthenium (II) as an electron donor and bipyridinium ions as electron acceptors have been extensively investigated⁶ and they provide an excellent model for demonstrating the role of zeolitic hosts

in photochemical charge separation. Several studies have focused on the steady-state photochemistry of trisbipyridine ruthenium (II) and bipyridinium ions in zeolites, demonstrating the possibilities for long-term charge separation.⁷ However, there are only three studies that have investigated the kinetics of the photoelectron transfer process for this system using time-resolved diffuse reflectance (TRDR) spectroscopy. Two of these studies are work by Mallouk and co-workers involving methyl viologen molecules in the cages of the zeolite and the $\text{Ru}(\text{bpy})_3^{2+}$ moiety on the zeolite surface.^{8a,b} They observed that the back electron transfer rate constant on the zeolite surface is considerably slower than that for comparable systems in solution. We reported results on the totally intrazeolitic $\text{Ru}(\text{bpy})_3^{2+}$ –methyl viologen system by monitoring a single wavelength at 610 nm for the decay of the viologen radical.^{8c}

In this paper, we expand on our earlier study by investigating the photoelectron transfer for a series of 2,2'-bipyridinium ions and methyl viologen, the structures of which are shown in Table

TABLE 1: 2,2'- and 4,4'-Bipyridinium Ions Used as Electron Acceptors

STRUCTURE	ABBREV.	E° (V) ^a	Δ E° (V) ^b
	2DQ ²⁺	-0.37	1.63
	MV ²⁺	-0.44	1.70
	3DQ ²⁺	-0.55	1.81
	4DQ ²⁺	-0.65	1.91

^a Volts vs NHE (ref 20). ^b The value E° (Ru³⁺/Ru²⁺) = 1.26 V (vs NHE) was used in this calculation.

1. Because of the varying reduction potentials of these electron acceptors, the driving force for intrazeolitic photochemical electron transfer with Ru(bpy)₃²⁺ could be modified. Electron transfer dynamics were measured using TRDR spectroscopy at wavelengths between 340 and 460 nm. Since the bipyridinium radicals have strong absorption bands in this region as compared to the visible region, the analysis of the time-resolved diffuse reflectance data presented in this study is considerably more detailed and leads to a more complicated picture than previously proposed.^{8c} The dynamics of the electron transfer at different loading levels of bipyridinium ions in the zeolite show distinct behavior. We find that the back electron transfer in the zeolite from the bipyridinium radical to Ru(bpy)₃³⁺ is smaller by several orders of magnitude as compared to the forward reaction. At low loadings of the bipyridinium ions, the rate of back electron transfer decreases with increasing driving force, as expected for reactions occurring in the Marcus inverted region. In the high loading case for all the electron acceptors studied, the migration of the photogenerated electron via hopping among adjacent bipyridinium molecules away from the ruthenium center leads to long-lived charge separation. For example, in the methyl viologen case, about 30% of the viologen radical signal formed during the laser pulse (15 ns) is present after 1 ms. A kinetic model is developed to explain these results, and the possible roles of the zeolite structure in slowing the back electron-transfer reaction are discussed.

Experimental Section

Synthesis of intrazeolitic Ru(bpy)₃²⁺ (loading level of 1 per 15 supercages) was done using previously described procedures.⁹ Methyl viologen (MV²⁺, Aldrich) was purified by crystallization from methanol/acetone. The remaining diquat ions were prepared as indicated in the literature.¹⁰ Elemental analysis and NMR spectroscopy confirmed the purity of the diquat ions. For the low loading samples of bipyridinium ions (1 ion in 10–15 supercages), Ru(bpy)₃²⁺–Y was ion-exchanged for 24 h with the exact concentrations of these ions to obtain the desired loadings. For the high loading samples, 100 mg of Ru(bpy)₃²⁺–Y was ion-exchanged overnight with 2 mL of a 0.1 M solution of the bipyridinium ion. Loading levels were determined by analyzing the supernatant solutions after ion-

exchange by absorption spectroscopy. For time-resolved diffuse reflectance studies, 25 mg of Ru(bpy)₃²⁺–viologen-zeolite Y was transferred to a NMR tube and suspended in 0.5 mL of water. The suspensions were deaerated by successive freeze–pump–thaw cycles and sealed under vacuum.

Fluorescence spectra were collected on a Spex Fluorolog instrument. Absorption and diffuse reflectance spectra were obtained with a Shimadzu UV 265 instrument, equipped with a Harrick diffuse reflectance attachment. Time-resolved diffuse reflectance measurements were made at time delays up to 10 ms after sample excitation. The excitation source was the second harmonic (532 nm) of a Quantel Nd:YAG Q-switched laser (15 ns pulse width; 1 Hz repetition), with pulse power of 21–24 mW. A 250 W pulsed Xenon lamp from Applied Photophysics was used as monitoring light. Diffusely reflected light was collected and focused into a SPEX 1877 Triplemate spectrometer (150 gr/mm gratings) and detected with a EG&G Princeton Applied Research photodiode array. Timing of the laser pulse, lamp pulse, time delay, and detection window (100 ns) was done with a EG&G high voltage pulse generator and a timing box for triggering the Q-switch and lamp pulse.

Modeling of the kinetic data was done using STELLA Research, a system dynamics modeling software from High Performance Systems, Inc., Hanover, NH. STELLA can be used to numerically simulate and predict time-dependent behavior of complex phenomena by constructing compartmental models. The software converts the coupled differential equations which describe the system into finite difference equations, which are solved with an appropriate time interval. The simulation results were compared with the experimental data visually for the best fits, since STELLA is not equipped with fitting routines. Molecular models for zeolites,^{11a} Ru(bpy)₃²⁺,^{11b} and the methyl viologen ions^{11c} were generated using previously published crystallographic data¹¹ on an IBM RISC System/6000 computer, with the program Cerius², developed by BIOSYM/Molecular Simulation.

Results

I. Ru(bpy)₃²⁺–Zeolite Y. The synthesis procedure of Ru(bpy)₃²⁺ in zeolite Y followed here has been described in the literature.⁹ The loading level chosen for this study is 1 Ru(bpy)₃²⁺ in 15 supercages. In zeolite Y, each supercage is surrounded by four supercages. If, as is expected, the distribution of 1 Ru(bpy)₃²⁺ in 15 supercages is random, then 1 in 5 Ru(bpy)₃²⁺ has another Ru(bpy)₃²⁺ in a neighboring supercage and three empty supercages, whereas for the rest of the Ru(bpy)₃²⁺ molecules, all the neighboring supercages are empty.¹²

Figure 1 shows the emission spectrum of Ru(bpy)₃²⁺–zeolite Y, and it is similar to that reported in the literature.^{8c,9} Transient diffuse reflectance spectrum of Ru(bpy)₃²⁺–zeolite Y excited with a 15 ns, 532 nm pulse and collected after 100 ns is shown in Figure 2a. There is a depletion of intensity of the band at 450 nm, assigned to the metal-to-ligand charge transfer band of Ru(bpy)₃²⁺. The band at 370 nm arises from the ligand-centered transition of Ru(bpy)₃^{2+*}, and resembles the spectrum of the 2,2'-bipyridine radical anion.¹³ The decrease in intensity of this band with time is a measure of the lifetime of the photoexcited state. Figure 3a shows a fit of the data at 370 nm as a function of time to a single-exponential decay with a rate constant of 1.5 × 10⁶ s⁻¹, which corresponds to an excited state lifetime of 0.67 μs. The lifetime determined from the emission spectral decay monitored at 610 nm for a completely hydrated Ru(bpy)₃²⁺–zeolite Y sample is 0.62 μs. Previous reports in the literature^{8a} have also noted differences between the lifetimes

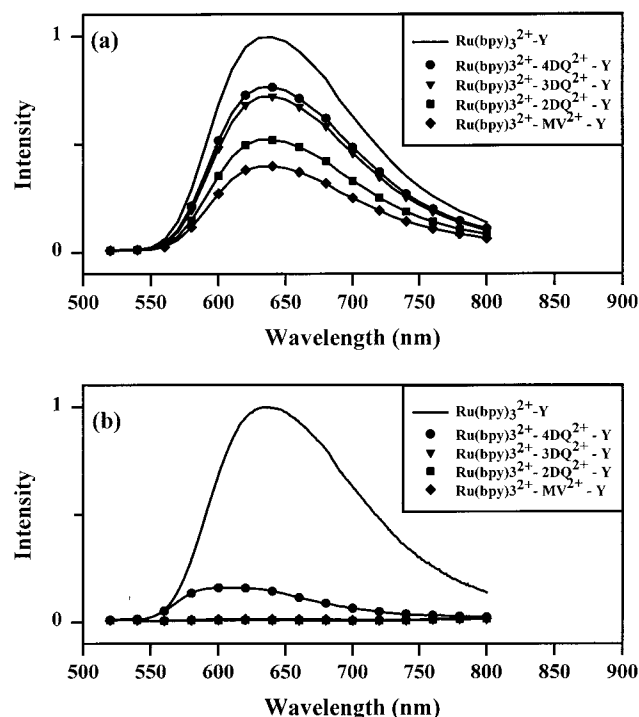


Figure 1. Emission spectra of (a) $\text{Ru}(\text{bpy})_3^{2+}$ -Y and with MV^{2+} , 2DQ^{2+} , 3DQ^{2+} , and 4DQ^{2+} at loadings of 1/15 supercage (b) $\text{Ru}(\text{bpy})_3^{2+}$ -Y and with high loadings of MV^{2+} , 2DQ^{2+} , 3DQ^{2+} , and 4DQ^{2+} (excitation wavelength = 450 nm).

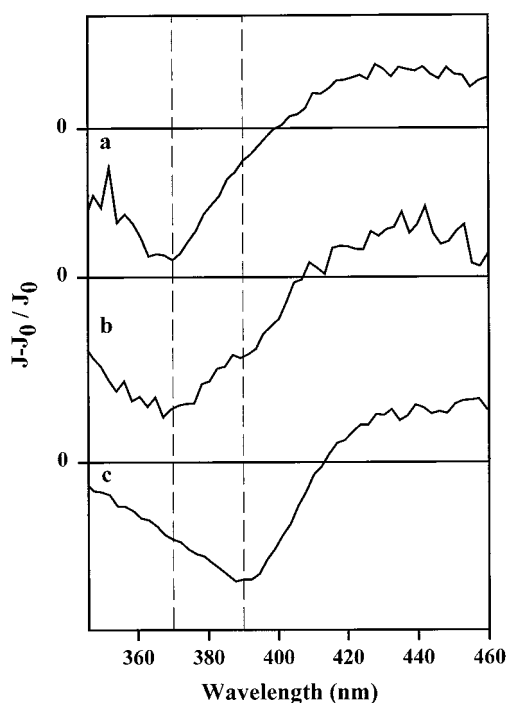


Figure 2. Comparison of TRDR spectra (100 ns after laser pulse) of (a) $\text{Ru}(\text{bpy})_3^{2+}$ -Y, (b) low loading $\text{Ru}(\text{bpy})_3^{2+}$ - MV^{2+} (1 per 15 supercages)-Y, and (c) high loading $\text{Ru}(\text{bpy})_3^{2+}$ - MV^{2+} (1.7 per supercage)-Y.

determined from transient absorption and emission spectra of $\text{Ru}(\text{bpy})_3^{2+}$ on zeolites and is a reflection of the experimental error.

II. Studies with Bipyridinium Electron Acceptors. The bipyridinium electron acceptors examined in this paper are shown in Table 1, along with their structures and the reduction potentials. Three of these acceptors are based on the 2,2'-

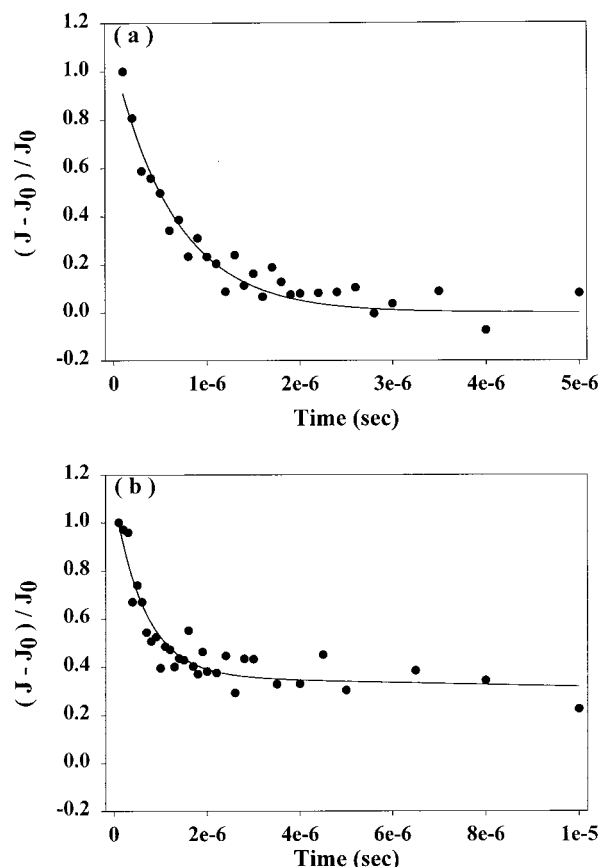
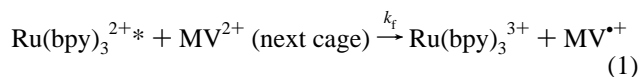


Figure 3. Decay of the transient diffuse reflectance signal at (a) 370 nm for $\text{Ru}(\text{bpy})_3^{2+}$ -Y and at (b) 389 nm for $\text{Ru}(\text{bpy})_3^{2+}$ - MV^{2+} (1 per 15 supercages)-Y. The solid lines through the data are fits to the data.

bipyridinium moiety, and their reduction potentials are controlled by the length of the connecting methylene chain units.¹⁴ These 2,2'-bipyridinium ions belong to the diquat family and are abbreviated in this study as $n\text{DQ}^{2+}$. The fourth viologen is the 1,1'-dimethyl-4,4'-bipyridinium (methyl viologen, MV^{2+}). The bipyridinium ions can be readily ion-exchanged into the $\text{Ru}(\text{bpy})_3^{2+}$ -zeolite Y. Since $\text{Ru}(\text{bpy})_3^{2+}$ completely fills a supercage, the bipyridinium ions must be in supercages not occupied by $\text{Ru}(\text{bpy})_3^{2+}$ molecules. We present the data with two extreme loadings of bipyridinium ions, a low loading of 1 in 15 or 1 in 10 supercages, and a high loading of 1.2–1.7 molecules per supercage.

a. Low Viologen Loadings. Figure 1a compares the fluorescence spectrum of $\text{Ru}(\text{bpy})_3^{2+}$ -zeolite Y with the corresponding bipyridinium ion loaded samples, at loading levels of 1 in 15 supercages. This low loading results in only a fraction of the $\text{Ru}(\text{bpy})_3^{2+}$ molecules in the zeolite being surrounded by bipyridinium ions. For those $\text{Ru}(\text{bpy})_3^{2+}$ molecules that have a bipyridinium ion in a neighboring supercage, oxidative quenching as exemplified below with MV^{2+} can occur (reaction 1).



However, since not all of the $\text{Ru}(\text{bpy})_3^{2+}$ molecules have a bipyridinium ion in the next supercage, the quenching of the $\text{Ru}(\text{bpy})_3^{2+*}$ is only partial and is reflected in the emission quenching shown in Figure 1a. This is also evident from Figure 2b which is the transient diffuse reflectance data for the $\text{Ru}(\text{bpy})_3^{2+}$ - MV^{2+} -zeolite sample, 100 ns after the laser pulse. There is the band at 370 nm due to the $\text{Ru}(\text{bpy})_3^{2+*}$ along with

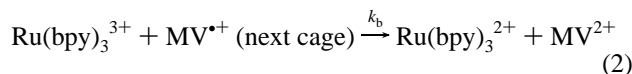
TABLE 2: Rate Constants in the Ru(bpy)₃²⁺–Bipyridinium–Zeolite Y System

viologen	low loading		high loading			
	loading ^a	<i>k_b</i> ^{ll} (s ^{−1})	loading ^a	<i>k_b</i> ^{hl} (s ^{−1})	<i>k_{hop}</i> (s ^{−1})	<i>k₂</i> (conc ^{−1} s ^{−1})
2DQ ²⁺	1/15	4.0 × 10 ⁴	1.6/1	2.5 × 10 ⁵	2.5 × 10 ⁵	6.0 × 10 ³
MV ²⁺	1/15	1.7 × 10 ⁴	1.7/1	9.0 × 10 ⁴	2.0 × 10 ⁵	3.0 × 10 ³
3DQ ²⁺	1/10	1.1 × 10 ⁴	1.4/1	1.8 × 10 ⁵	2.3 × 10 ⁵	1.0 × 10 ³
4DQ ²⁺	1/10	7.3 × 10 ³	1.2/1	1.2 × 10 ⁵	1.8 × 10 ⁵	1.5 × 10 ³

^a Loading indicates viologen molecules per supercage; ll = low loading; hl = high loading.

a shoulder around 389 nm due to the MV^{•+}.¹⁵ Similar experiment with an aqueous slurry of MV²⁺–zeolite sample showed no evidence for formation of MV^{•+}.

The signal due to MV^{•+} decays with time as a result of the back electron transfer to Ru(bpy)₃³⁺ (reaction 2).



To measure the rate of the back electron transfer, we fitted the decay at two wavelengths around the observed maximum of the absorption band of MV^{•+} (387, 389 nm) to a sum of two exponentials. One of the two exponentials has the decay rate constant of 1.5 × 10⁶ s^{−1}, characteristic of the Ru(bpy)₃²⁺* molecule isolated from interaction with bipyridinium ions, and was held constant for the fit. The other exponential provided the measure of the rate of the back electron transfer reaction. Figure 3b shows the decay of the intensity at 389 nm and the corresponding fit by a double-exponential function (detailed plot in the Supporting Information). The back electron transfer rate constant *k_b*^{ll} (ll = low loading) obtained for the two wavelengths was averaged and found to be 1.7 × 10⁴ s^{−1}. In a similar fashion, *k_b*^{ll} for 2DQ²⁺ at a loading level of 1 in 15 supercages was determined to be 4.0 × 10⁴ s^{−1} by monitoring the decay at wavelengths of 374, 376, and 379 nm. For 3DQ²⁺ and 4DQ²⁺, the loading level of 1 in 15 supercages was insufficient to create enough bipyridinium radical to noticeably perturb the transient diffuse reflectance spectrum and it resembled that of Ru(bpy)₃²⁺*–zeolite. For these two bipyridinium ions, the loading level was increased to 1 in 10 supercages. At this loading level, back electron transfer rate constants of 1.1 × 10⁴ and 7.3 × 10³ s^{−1} were found for 3DQ²⁺ and 4DQ²⁺, respectively, by monitoring wavelengths at 379, 381, and 383 nm for 3DQ²⁺ and 374, 376, and 379 nm for 4DQ²⁺. These values are listed in Table 2.

b. High Loading Levels. The highest loading levels obtained for 2DQ²⁺, MV²⁺, 3DQ²⁺, and 4DQ²⁺ were 1.6, 1.7, 1.4, and 1.2 molecules per supercage. Figure 1b shows that the quenching of the Ru(bpy)₃²⁺* emission by the bipyridinium ions is efficient and follows the order MV²⁺ > 2DQ²⁺ > 3DQ²⁺ > 4DQ²⁺, with the magnitude of quenching (defined as *I₀/I*) being 108, 103, 67, and 6 for MV²⁺, 2DQ²⁺, 3DQ²⁺, and 4DQ²⁺, respectively. The efficient quenching is also reflected in the transient diffuse reflectance data. As an example, Figure 2c shows the diffuse reflectance spectra 100 ns after the laser pulse for a high loading Ru(bpy)₃²⁺–MV²⁺–zeolite Y. Comparison to Figure 2a shows that the peak maximum has changed from 370 to 390 nm. This arises because the Ru(bpy)₃²⁺* is completely quenched by MV²⁺ and the signal present is due to the MV^{•+} radical absorption band at 390 nm.¹⁵ Similar results were also observed with the high loading nDQ²⁺ samples. Quantitative information about the dynamics of the forward electron transfer could not be obtained via TRDR. Within the first 100 ns window of measurement (minimum time for which the detector gate is left open), the signal for the bipyridinium

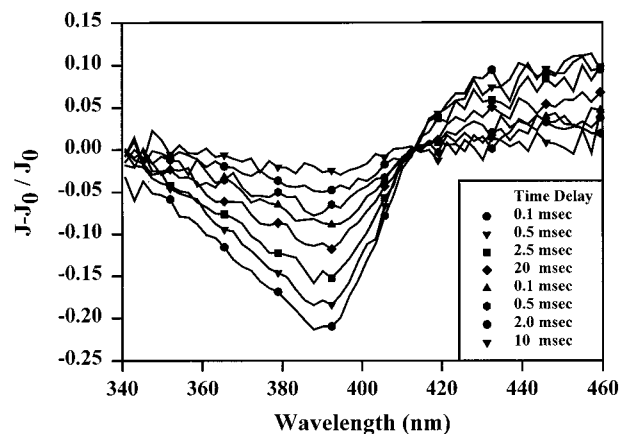
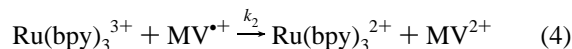
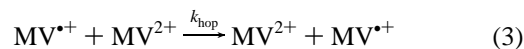


Figure 4. Time-resolved diffuse reflectance (TRDR) spectra of high loading Ru(bpy)₃²⁺–MV²⁺ (1.7 per supercage)–Y.

ion radicals is maximized, indicating that the forward rate constant is greater than 10⁷ s^{−1}.

The dynamics of the back electron transfer (reaction 2) was obtained by monitoring the decay of the bipyridinium radical signal as a function of time. Figure 4 shows representative time-resolved diffuse reflectance (TRDR) spectra of the high loading Ru(bpy)₃²⁺–MV²⁺ (1.7 molecule per supercage)–zeolite in the wavelength range of 340–460 nm. The data points in Figure 5a are the intensity of the MV^{•+} signal (389 nm) as a function of time. In the high loading case, the bipyridinium radical signal was longer-lived by several orders of magnitude compared to the low loading sample and did not follow a monoexponential decay. This observation was consistent for all four electron acceptors. Figure 5 is a comparison of the decay of the bipyridinium radical for all the high loading samples. The insets in the figure show the data at shorter times.

A more complicated model was developed to describe the decay behavior of the high loading samples. We have included the following additional reactions at high loading levels (using MV²⁺ as the example):



Electron hopping between bipyridinium ions (*k_{hop}*) provides a pathway (reaction 3) for the electron to move farther away from the Ru(bpy)₃³⁺ center. Once the electron has hopped on to neighboring cages, it can “diffuse” around in the zeolite via charge hopping until it encounters a Ru(bpy)₃³⁺. This recombination process is represented in reaction 4 and is controlled by *k₂*, a second-order rate constant.

The solid lines through the decay in Figure 5 are the simulated fits using this model. There are three rate constants involved in the process: *k_b*^{hl} (hl high loading), *k_{hop}*, and *k₂*. The following strategy was used to determine the values of these rate constants. First, *k_b*^{hl} was estimated by numerically fitting the bipyridinium

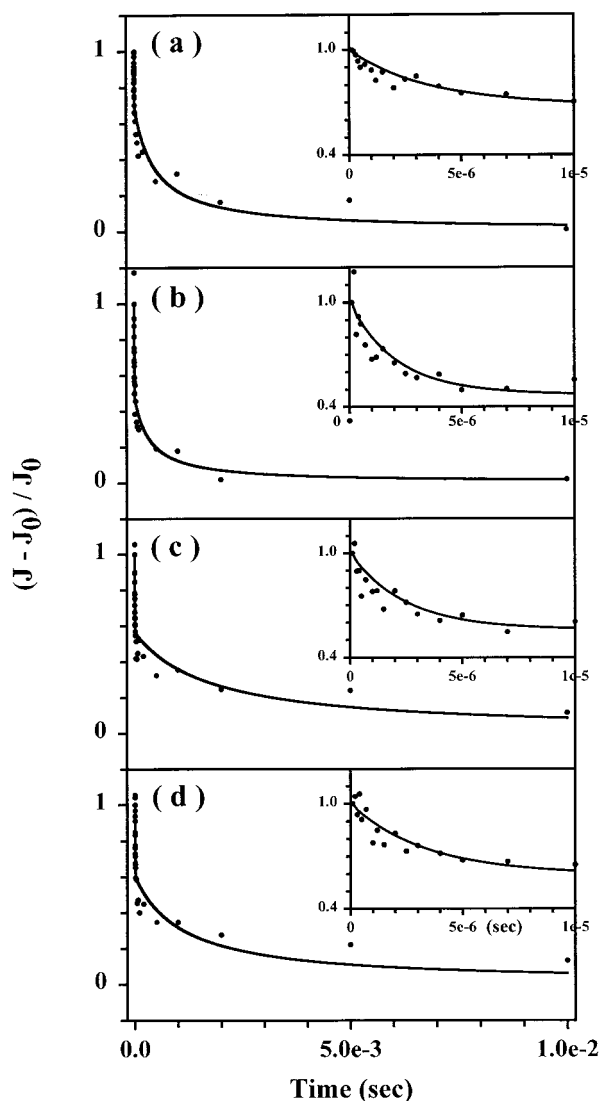


Figure 5. Plot of the decay of the bipyridinium radical ion signal for high loading bipyridinium– $\text{Ru}(\text{bpy})_3^{2+}$ –Y (insert shows the decay at shorter times): (a) MV^{2+} , (b) 2DQ^{2+} , (c) 3DQ^{2+} , (d) 4DQ^{2+} . Solid lines are fits to the data using the model described in the paper.

radical ion decay for time intervals $< 1 \mu\text{s}$. Similarly, k_2 was estimated by fitting the same decay at time intervals $> 10 \mu\text{s}$. These values were then used to initiate the kinetic model and the decay was simulated using STELLA. The simulation results were compared with the experimental data visually for the best fit and the corresponding k_b^{hl} , k_2 , and k_{hop} are reported in Table 2. To convert k_2 to concentration units, the absorptivity of the bipyridinium radical ion inside the zeolite and the penetration depth need to be known. Previous studies have considered the absorptivity of viologen in the zeolite to be the same as in solution and is a reasonable approximation.^{8b} However, the penetration depth is not readily determined and so we are not reporting k_2 in more conventional units. The back electron transfer rates are higher in magnitude as compared to the low loading bipyridinium samples and follow the order $2\text{DQ}^{2+} > 3\text{DQ}^{2+} > 4\text{DQ}^{2+} > \text{MV}^{2+}$.

In the case of MV^{2+} , we also estimated a transient quantum yield of formation of $\text{Ru}(\text{bpy})_3^{3+}$ and $\text{MV}^{\bullet+}$ 100 ns after the excitation pulse, and is determined to be between 0.44 and 0.59 (multiple measurements). This was done by estimating the absolute $(J - J_0)/J_0$ values from parts a and c of Figure 2. Two assumptions were needed to get the quantum yield. First, the molar absorptivities of the viologen radical (389 nm) and

$\text{Ru}(\text{bpy})_3^{2+*}$ (370 nm) were taken to be $42100 \text{ L mol}^{-1} \text{ cm}^{-1}$ and $27300 \text{ L mol}^{-1} \text{ cm}^{-1}$, respectively, the same as in solution.^{16,17} Second, the penetration depth of the radiation was considered to be similar for both $\text{Ru}(\text{bpy})_3^{2+}$ –zeolite Y and $\text{Ru}(\text{bpy})_3^{2+}$ –bipyridinium–zeolite Y. These assumptions were similar to previous studies in the literature.^{8b} Also, no correction factors were applied for differences in penetration depths at wavelengths 390 and 370 nm, considering that these wavelengths are close to each other.¹⁸ Since the absorptivities of the $n\text{DQ}^{\bullet+}$ radical ions are not well-established, we did not estimate the quantum yields for the diquat systems.

A more meaningful parameter from the charge utilization point of view is a zeolite supercage escape yield. This is defined as the fraction of bipyridinium ion radicals that no longer have $\text{Ru}(\text{bpy})_3^{3+}$ in a neighboring cage and is $k_{\text{hop}}/(k_{\text{hop}} + k_b)$, which amounts to about 0.69 for the high loading $\text{Ru}(\text{bpy})_3^{2+}$ – MV^{2+} –zeolite Y. Similar calculations for 2DQ^{2+} , 3DQ^{2+} , and 4DQ^{2+} result in zeolite supercage escape yields of 0.50, 0.56, and 0.60, respectively. For the low loading samples, such a cage escape yield would be zero since there is no charge propagation out of the supercage in which the bipyridinium radical ion was generated.

Discussion

Figure 6a shows a cross section of a zeolite crystal comprising of three supercages. In the left cage is a molecule of $\text{Ru}(\text{bpy})_3^{2+}$, and it occupies most of the volume of the supercage. These structures are based on crystallographic data for zeolite Y and $\text{Ru}(\text{bpy})_3^{2+}$.¹¹ A large number of orientations of $\text{Ru}(\text{bpy})_3^{2+}$ in a supercage are obviously possible. The modeling program provides the interatomic distances between the atoms of $\text{Ru}(\text{bpy})_3^{2+}$ molecule and the surrounding zeolite framework. We designate a “bad” contact as one where two atoms approach each other at less than 90% of the sum of their van der Waals radii.¹⁹ For every orientation of $\text{Ru}(\text{bpy})_3^{2+}$ that we have examined, there are several such bad contacts, usually between the H or C atoms of $\text{Ru}(\text{bpy})_3^{2+}$ and the oxygen atoms of the zeolite framework. In some cases, bad contacts are also observed with the Si atoms of the framework (figure shown in Supporting Information). Of course, the manual search that we perform does not exhaust all the possible orientations. Nevertheless, the presence of these bad contacts suggests that though it is possible to synthesize $\text{Ru}(\text{bpy})_3^{2+}$ within a supercage, the rotational mobility of the $\text{Ru}(\text{bpy})_3^{2+}$ will be restricted in the zeolite.

Upon ion-exchanging bipyridinium ions into the zeolite, they fill the empty supercages. At low loading levels of 1 bipyridinium ion in 10–15 supercages, the probability of more than one bipyridinium ion in a supercage is practically zero. Figure 6b shows a MV^{2+} ion in a cage neighboring that of $\text{Ru}(\text{bpy})_3^{2+}$, and it appears that there is considerable room for MV^{2+} to move around in the supercage. Crystallographic data was used to generate the MV^{2+} structure.^{11c} Figure 6c shows the packing of methyl viologen under high loading conditions, which corresponds to little over three methyl viologen molecules in two cages. This is obviously one of the many arrangements that are possible. The figure is meant to reflect the crowding of the MV^{2+} in the supercages, the low mobility, and the close approach of these molecules upon high loading. In the case of the diquats, the loadings were slightly lower though comparable (Table 2). In the high loading case, the $\text{Ru}(\text{bpy})_3^{2+}$ is also surrounded by the bipyridinium ions in all four neighboring supercages.

I. Quenching of $\text{Ru}(\text{bpy})_3^{2+*}$. The oxidative quenching of intrazeolitic photoexcited $\text{Ru}(\text{bpy})_3^{2+}$ occurs by electron transfer

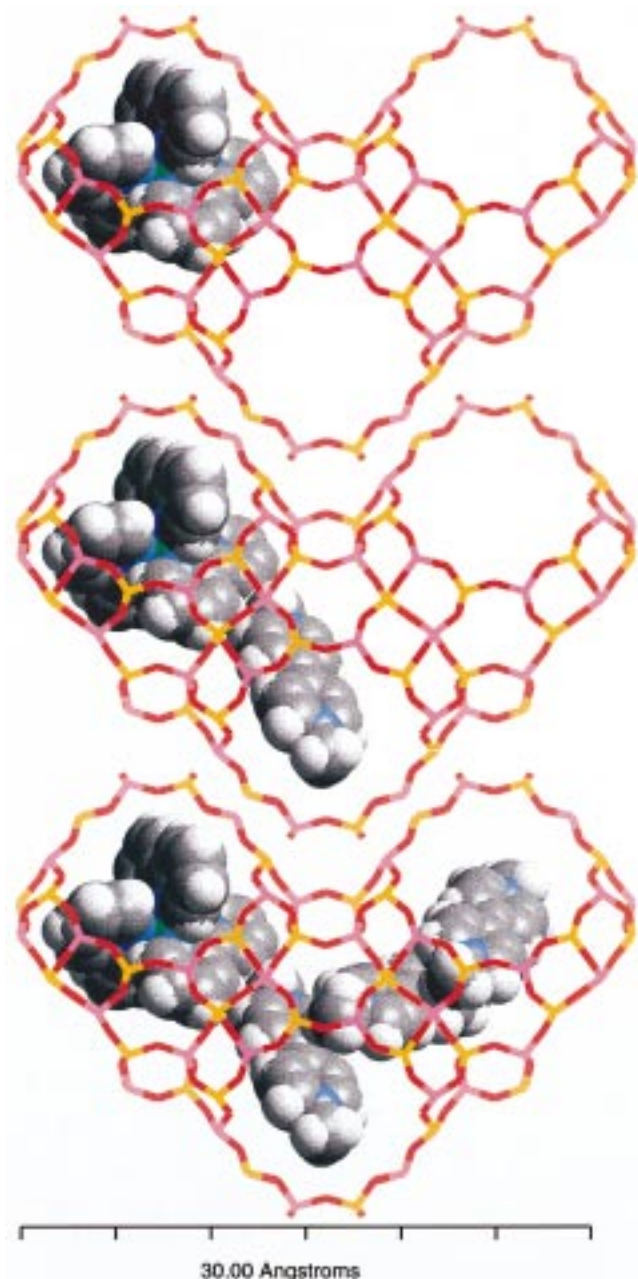


Figure 6. Geometric arrangement of $\text{Ru}(\text{bpy})_3^{2+}$ in a zeolite supercage (top) and methyl viologen in a low loading sample (middle) and high loading sample (bottom).

to bipyridinium ions. The emission spectral data in Figure 1 shows that, at both low and high loading levels, the quenching follows the order $\text{MV}^{2+} > 2\text{DQ}^{2+} > 3\text{DQ}^{2+} > 4\text{DQ}^{2+}$. The electron transfer quenching of $\text{Ru}(\text{bpy})_3^{2+}$ by several bipyridinium ions in solution has been examined, and the quenching rate constants are found to increase as the bipyridinium reduction potentials become less negative.^{20,21} For the diquat ($n\text{DQ}^{2+}$) series reported here, the order of quenching is as is expected from the reduction potentials, indicating that as the driving force for the forward electron transfer decreases, the propensity to quench the intrazeolitic $\text{Ru}(\text{bpy})_3^{2+}$ by electron transfer also decreases. The reduction potential of methyl viologen is between that of 2DQ^{2+} and 3DQ^{2+} , yet it quenches $\text{Ru}(\text{bpy})_3^{2+}$ most efficiently.

In the zeolite, the diffusional contribution to electron-transfer quenching is expected to be small. The bipyridinium ions will need to diffuse through the 7 Å windows, and considering that

the lateral width of the smallest of these molecules is 6.3 Å, intercage diffusion is likely to be slow. In the high loading samples, the bipyridinium ions are considerably more constrained, since the whole zeolite crystallite is packed with the bipyridinium ions. Because of these diffusional limitations, the quenching of intrazeolitic $\text{Ru}(\text{bpy})_3^{2+}$ is more of a static process, and photochemical electron transfer is occurring between $\text{Ru}(\text{bpy})_3^{2+}$ in a supercage with the bipyridinium molecules in only the neighboring supercages. Kim and Mallouk have reported that if the $\text{Ru}(\text{bpy})_3^{2+}$ is ion-exchanged on the zeolite surface and MV^{2+} is in the zeolite, then the quenching process is primarily dynamic.^{8a} Thus, constraining the $\text{Ru}(\text{bpy})_3^{2+}$ inside the zeolite has an effect on the nature of the quenching process.

For the high loading bipyridinium systems, the rate constant for quenching (k_f) is $> 10^7 \text{ s}^{-1}$. The exact rate constants could not be determined due to limited time resolution of the instrument. However, both the lower limit of 10^7 s^{-1} for the rate constant and the emission quenching data indicate that the oxidative quenching is efficient. There are several reasons for the effective quenching. The cage structure of the zeolite and the packing of the bipyridinium ions limits the distance between the Ru center and the bipyridinium ions (Figure 6). For covalently linked $\text{Ru}(\text{bpy})_3^{2+}$ –viologen systems, the forward electron transfer rate constants are slowed upon ion-exchanging onto the surface of zeolites or colloidal aluminosilicate particles.^{8b,22,23} The slowing down of the electron transfer on adsorption has been proposed as due to restricted conformational arrangements.^{8b} In the case of intrazeolitic quenching, the influence of conformational limitations is going to be insignificant since each $\text{Ru}(\text{bpy})_3^{2+}$ is surrounded by bipyridinium ions on four sides as compared to only one edge for covalently held complexes. In modeling rotational arrangements of $\text{Ru}(\text{bpy})_3^{2+}$ in the supercage, two of the bpy ligands are always found to be positioned facing two of the four 7 Å cage windows (Figure 6). It is generally agreed that, in the MLCT state, the electron is localized on the bipyridine ligand,²⁴ and thus the forward electron transfer can occur from the $\text{bpy}^{\bullet-}$ to a bipyridinium ion readily across the 7 Å window.

II. Back Electron Transfer from Bipyridinium Radical Ion to $\text{Ru}(\text{bpy})_3^{3+}$ in the Zeolite. There are several issues that are related to the back electron transfer rate constants. These include the dependence of the back electron transfer rate constants on the viologen loading levels, the decreased value of the back electron-transfer rate constants in the zeolite as compared to the forward electron transfer and the dependence of the back electron transfer rate constant on the bipyridinium reduction potential.

a. Loading Effects. There are two sets of back electron transfer rate constants reported in Table 2 determined by the loading of the bipyridinium ions into the zeolite. The low loading samples have rate constants that are smaller by a factor of 10 as compared to the high loading samples. In the low loading case (Figure 6b), a supercage at most only contains one bipyridinium ion. This provides the bipyridinium radical ion the possibility of exploring the volume of the supercage leading to greater separation between the $\text{Ru}(\text{bpy})_3^{3+}$ and the radical ion. In the high loading case, as is evident from Figure 6, the bipyridinium ions are closer to the $\text{Ru}(\text{bpy})_3^{2+}$ and their mobility is considerably restricted since the whole zeolite crystallite is filled with bipyridinium ions. Thus, the separation distance between the $\text{Ru}(\text{bpy})_3^{3+}$ and the bipyridinium radical ion is smaller on average in the high loading case and should result in a faster back electron transfer reaction.

b. Magnitude of the Back Electron Transfer Reaction Rate Constants. In the intrazeolitic $\text{Ru}(\text{bpy})_3^{2+}$ –bipyridinium samples, there appears to be at least a 2 orders of magnitude decrease in the back versus forward electron transfer rate constants. Considerable research has been done on the $\text{Ru}(\text{bpy})_3^{2+}$ –viologen and $\text{Ru}(\text{bpy})_3^{2+}$ –diquat systems in solution and on various matrixes.^{4,25,26} In the covalently held Ru–viologen or Ru–diquat complexes, the rate constants for the back electron transfer reaction are comparable or slightly faster than the forward electron transfer and the orders of magnitude are 10^{10} s^{-1} .²¹ In solution, the forward electron transfer is diffusion controlled and the back electron-transfer typical of the geminate recombination of $\text{Ru}(\text{bpy})_3^{3+}$ and viologen radicals is also of the order of 10^{10} s^{-1} .²⁷ If the $\text{Ru}(\text{bpy})_3^{2+}$ and viologen are held in micelles, then the rate constant for the back electron transfer was reported as $5.7 \times 10^6 \text{ s}^{-1}$, and the forward electron transfer rate constant was not reported.²⁸ If covalently held $\text{Ru}(\text{bpy})_3^{2+}$ –viologen complexes are adsorbed on alumina-coated colloidal silica particles, nanosecond transient studies suggest that the back electron transfer is faster than the forward reaction.²³ Only in the case of $\text{Ru}(\text{bpy})_3^{2+}$ –viologen ion-exchanged onto surface zeolite sites via the charged viologen moiety, there was a significant increase in the lifetime of charge separated species reported.^{8b} It was proposed that lateral charge transfer between Ru and/or viologen centers was occurring on the zeolite surface. However, in the present study, k_b ^{ll} was determined from low loading samples of bipyridinium ions, which essentially contained isolated $\text{Ru}(\text{bpy})_3^{2+}$ –viologen units separated spatially from each other and there is no opportunity for lateral charge transfer. Thus, the differences between the forward and back electron transfer rate constants for reactions within the zeolite must be due to the role of the framework.

The rates of electron transfer are controlled by the exoergicity of the reaction, the reorganization energy, adequate spin–orbit coupling for triplet to singlet conversion in the back electron transfer process, and appropriate orbital overlap between donor and acceptor. How these factors are influenced by zeolite encapsulation is not yet known. We discuss briefly some general observations in this regard.

Electrochemistry on zeolite Y modified electrodes shows that at loadings of 1 viologen per 2 supercages, the redox potentials of different viologens are close to the values in solution.²⁹ Electrochemical studies on $\text{Ru}(\text{bpy})_3^{2+}$ ion-exchanged on the surface of zeolite Y show shifts in the redox potential to more positive values,³⁰ decreasing the driving force for the forward electron transfer quenching with bipyridinium ions. Thus, it was found that the quenching of $\text{Ru}(\text{bpy})_3^{2+*}$ emission on the surface of the zeolite by 3DQ^{2+} was poor.^{7a} However, as shown in Figure 1b, the decrease of intrazeolitic $\text{Ru}(\text{bpy})_3^{2+*}$ emission upon 3DQ^{2+} quenching is greater than a factor of 60 and resembles that observed in solution. Thus, even though the values of the reduction potentials inside the zeolite are not known, the similarities that are observed for quenching reactions in the zeolite and in solution for comparable systems indicate that the reduction potentials inside the zeolite are not being altered dramatically.

The influence of the solvent reorganization energy in zeolites on the electron transfer dynamics is difficult to evaluate since the intrazeolitic solvation environment is not well studied. In the high loading bipyridinium case, there could be a parallel to previous observations in rigid/frozen media. Solvent molecules cannot reorient in these media and profound effects on electron-transfer dynamics are observed.^{31,32} In a zeolite sample, water

molecules are coordinated to ions, as well as there is bulk water in the supercages.³³ As molecules such as $\text{Ru}(\text{bpy})_3^{2+}$ and bipyridinium ions fill the supercages, they replace the bulk water molecules, leaving behind proportionately increasing levels of water molecules that are strongly coordinated to the sodium cations and the zeolite framework and are less mobile.

The back electron transfer process is also accompanied by a spin inversion of the mostly triplet $\text{Ru}(\text{bpy})_3^{3+}$ –bipyridinium radical ion which is formed immediately after quenching to the singlet ground $\text{Ru}(\text{bpy})_3^{2+}$ –bipyridinium ion. The rotational motion of the $\text{Ru}(\text{III})$ complex promotes the triplet to singlet conversion.³⁴ Constraining the $\text{Ru}(\text{bpy})_3^{2+}$ in the zeolite supercage will disrupt the spin conversion pathway and can contribute to slowing of the back electron transfer reaction.

Modification of the extent of orbital overlap between the acceptor and donor can occur because of entrapment. Unlike the forward electron transfer that occurs from the bpy ligand to the bipyridinium ions across the 7 Å window, the back electron transfer needs to occur from the bipyridinium radical ion to the $d\pi$ (A_1) orbital of ruthenium,^{35a} in the center of the neighboring supercage. The $d\pi$ (A_1) orbital does not interact with the bpy ligand orbitals.^{35b} This will necessitate $\text{Ru}(\text{bpy})_3^{3+}$ reorienting inside the zeolite to allow for a favorable overlap of the metal and viologen orbitals. The likelihood of $\text{Ru}(\text{bpy})_3^{3+}$ rotating inside the supercage is negligible because of the steric constraints in the zeolite. The influence of orientational effects on electron transfer rates is well recognized in the literature.³⁶ Theoretical calculations of the electronic coupling between donor and acceptor sites for metallocene–metallocenium redox pairs have shown a striking dependence on their relative orientations.³⁷

Recently, an electron confinement concept for explaining altered chemical and photochemical reactivity in zeolites has been proposed³⁸ and is related to the orbital overlap argument just advanced. The negative charge of the zeolite is partially delocalized over the aluminosilicate framework that forms the walls of the cages. The electron density of the guest molecule orbitals that extend to the walls of the cages will be repelled by the electron cloud of the framework, leading to a spatial contraction of the orbitals. This effect will be pronounced for molecules that occupy the entire cage volume, such as $\text{Ru}(\text{bpy})_3^{2+}$. With this orbital contraction, the overlap of donor–acceptor orbitals, even for similar geometrical arrangements, will be different in the zeolite as compared to other media and will influence the back electron transfer reaction in the $\text{Ru}(\text{bpy})_3^{2+}$ –bipyridinium system more so than the forward reaction.

c. Relationship between Back Electron Transfer and Bipyridinium Ion Reduction Potentials. We will primarily discuss the high loading bipyridinium ion back electron transfer rate constants, since the geometry of the donor acceptor pairs are better defined because of the restricted mobility of the bipyridinium ions. The back electron-transfer rate constants between the different bipyridinium ions follow the order $2\text{DQ}^{2+} > 3\text{DQ}^{2+} > 4\text{DQ}^{2+} > \text{MV}^{2+}$. Based on the reduction potentials of the bipyridinium ions in solution, the driving force for the back electron-transfer reaction for this series is expected to be $2\text{DQ}^{2+} < \text{MV}^{2+} < 3\text{DQ}^{2+} < 4\text{DQ}^{2+}$. For the diquat series, the reactions follow the inverted behavior. Similar results have been reported for reaction of $\text{Ru}(\text{bpy})_3^{2+}$ with diquat ions in solution.²⁰ Covalently held $\text{Ru}(\text{bpy})_3^{2+}$ –viologen and diquat moieties also show behavior expected for reactions occurring within the inverted region.^{21a,c,22,39} Thus, the intrazeolitic behavior is consistent with previous studies.

However, MV²⁺ is not following the trend, the electron transfer rate being considerably slower from what would be expected from its reduction potential. In the case of MV²⁺, both the quenching of Ru(bpy)₃²⁺* and the back electron transfer from the viologen radical to Ru(bpy)₃³⁺ are not consistent with the prediction based on its reduction potential. The geometry of the MV²⁺ is quite distinct from the diquat ions. Its cylindrical shape allows for more efficient approach to Ru(bpy)₃²⁺. Also, as compared to the diquat series, where the rotation around the bipyridinium units is essentially controlled by the methylene units, there is no restraint on the twisting around the C–C bond in MV²⁺.

III. Longer-Lived Charge Separation in High Loaded Bipyridinium Samples. Despite the larger back electron-transfer rate constants for the high loading bipyridinium samples, long-lived charge-separated species are observed. Previous studies of Ru(bpy)₃²⁺ and MV²⁺, as well as the covalently linked Ru(bpy)₃²⁺–viologen samples on zeolite surfaces have shown that the recombination dynamics are complex.^{7,8} In the intrazeolitic study described here, the complexity in the back electron transfer dynamics for the high loading samples arises from the competition between back electron transfer and self-exchange processes. The model that we have used to explain long-lived charge separation is parallel to the processes that occur in solution,⁴⁰ with the difference being in the time scales, with events being slowed down in the zeolite and the packing of the bipyridinium ions making possible the charge migration in the zeolite.

The idea that self-exchange between viologens can lead to longer lived charge separation in surface reactions in zeolites was first noted by Mallouk and co-workers, based on transient spectroscopy.^{7a} We have used the self-exchange argument to help explain the steady-state charge separation observed on photolysis of Ru(bpy)₃²⁺–methyl viologen zeolite samples.^{8c} It is of interest to compare the dynamics of electron transfer as one proceeds from the surface of the zeolite to the bulk. For covalently held Ru(bpy)₃²⁺–viologen systems ion-exchanged onto the surface of zeolites, it was estimated that the electron exchange rate is about 10 times slower than the back electron-transfer reaction.^{8b} On the external surface of the (111) face of zeolite Y, the spacing between centers of the supercages is of the order of 11 Å. In the completely intrazeolitic Ru(bpy)₃²⁺–bipyridinium systems, the electron hopping rate constants are comparable to the back electron transfer rate constant. The dense packing of the bipyridinium ions in the intrazeolitic case leads to van der Waals contacts between the ions and thereby can promote more efficient charge hopping as compared to the external surface of the zeolite.

The zeolite Y topology should also aid in the charge separation process. As the electron escapes from the Ru(bpy)₃³⁺–bipyridinium radical ion assembly in adjacent cages to a neighboring supercage, it can return back to the same supercage. However, at this stage, it has the option of recombining with Ru(bpy)₃³⁺ in one of the cages, or moving to a bipyridinium ion in three of the other cages. This would not occur in zeolites with one-dimensional channels such as zeolite L or mordenite.

There have been several other instances where long-lived charge separation has been reported in zeolites, including charge transfer between arenes as electron donors and viologen as electron acceptors.⁴¹ Unlike the case presented here, where donors and acceptors are in neighboring cages, the arene and the viologen occupy the same cage. The reason for the long-lived charge separation was proposed to be electrostatic in

nature, where the arene cation and viologen radical ion are pulled to opposite ends of the supercage, thereby slowing down the electron transfer reaction.

Other examples of long-lived charge separation include cases where the zeolite framework is the electron donor. Thomas and co-workers have reported that pyrene anion radicals are formed by photochemical electron transfer from the zeolite.⁴² The special intrazeolitic environment is required for this reaction. No evidence of pyrene radicals are observed on the exterior of the zeolite. Scaiano and co-workers have noted that laser flash photolysis of MV²⁺–zeolite at 266/355 nm results in electron transfer from the framework and long-lived formation of the methyl viologen radical cation.⁴³ The rate of the back electron transfer was controlled by the framework basicity.

Conclusion

In conclusion, this study establishes that the zeolite framework has a significant role in influencing electron-transfer rates by virtue of the arrangement of acceptor and donor molecules. Forward electron transfer is favorable, while the back electron transfer is restricted. The mechanism by which the zeolite environment influences the reaction dynamics is yet to be evaluated. The rates of the back electron transfer decrease with increasing driving force for the reaction, indicating that the reactions are occurring in the Marcus inverted region. The favorable packing of the bipyridinium acceptor molecules via the ion-exchange properties of the zeolite also provides a pathway for the photogenerated electron to migrate via bipyridinium self-exchange, leading to long-term charge separation.

Acknowledgment. We acknowledge DOE, Division of Chemical Sciences for funding. Discussion with Professor T. J. Meyer helped clarify some issues for which we are grateful. Suggestions from Prof. G. C. McBane regarding modeling the kinetic data are appreciated. Mr. Ty Le has also helped clarify some of the discussions in this paper.

Supporting Information Available: Three figures. This material is available free of charge via the Internet at <http://pubs.acs.org>.

References and Notes

- (1) Khaselev, O.; Turner, J. A. *Science* **1988**, 280, 425.
- (2) Bard, A. J.; Fox, M. A. *Acc. Chem. Res.* **1995**, 28, 141.
- (3) Gust, D.; Moore, T. A.; Moore, A. L. *Acc. Chem. Res.* **1993**, 26, 198.
- (4) (a) Grätzel, M.; Kalyanasundaram, K., Eds. *Kinetics and Catalysis in Microheterogeneous Systems*; Marcel Dekker: New York, 1991. (b) Ramamurthy, V., Ed. *Photochemistry in Organized and Constrained Media*; VCH: New York, 1991.
- (5) Dutta, P. K.; Ledney, M. *Prog. Inorg. Chem.* **1997**, 44, 209.
- (6) Kalyanasundaram, K. *Photochemistry of Polypyridine and Porphyrin Complexes*; Academic Press: London, 1992.
- (7) (a) Krueger, J. S.; Mayer, J. E.; Mallouk, T. E. *J. Am. Chem. Soc.* **1988**, 110, 8232. (b) Borja, M.; Dutta, P. K. *Nature* **1993**, 362, 43. (c) Sykora, M.; Kincaid, J. R. *Nature* **1997**, 387, 162.
- (8) (a) Kim, Y. I.; Mallouk, T. E. *J. Phys. Chem.* **1992**, 96, 2879. (b) Yonemoto, E. H.; Kim, Y. I.; Schmehl, R. H.; Wallin, J. O.; Shoulders, B. A.; Richardson, B. R.; Haw, J. F.; Mallouk, T. E. *J. Am. Chem. Soc.* **1994**, 116, 10557. (c) Dutta, P. K.; Turbeville, W. J. *Phys. Chem.* **1992**, 96, 9410.
- (9) (a) De Wilde, W.; Peeters, G.; Lunsford, J. H. *J. Phys. Chem.* **1980**, 84, 2306. (b) Maruszewski, K.; Kincaid, J. R. *Inorg. Chem.* **1995**, 34, 2002.
- (10) Homer, R. F.; Tomlinson, T. E. *J. Chem. Soc.* **1960**, 2498.
- (11) (a) Olson, D. H. *J. Phys. Chem.* **1970**, 74, 2758. (b) Rillema, D. P.; Jones, D. S.; Woods, C.; Levy, H. A. *Inorg. Chem.* **1992**, 31, 2935. (c) Russell, J. H.; Wallwork, S. C. *Acta Crystallogr.* **1972**, B28, 1527.
- (12) Sykora, M.; Kincaid, J. R.; Dutta, P. K.; Castagnola, N. *J. Phys. Chem. B* **1999**, 103, 309.

- (13) (a) Lachish, U.; Infelta, P. D.; Grätzel, M. *Chem. Phys. Lett.* **1979**, 62, 317. (b) Creutz, C.; Chou, M.; Netzel, T. L.; Okumura, M.; Sutin, N. *J. Am. Chem. Soc.* **1980**, 102, 1309.
- (14) Willner, I.; Ayalon, A.; Rabinovitz, M. *New J. Chem.* **1990**, 14, 685.
- (15) (a) Yoshimura, A.; Hoffman, M. Z.; Sun, H. *J. Photochem. Photobiol. A* **1993**, 70, 29. (b) Evans, A. G.; Dodson, N. K.; Rees, N. H. *J. Chem. Soc., Perkin Trans.* **1976**, 2, 859.
- (16) Kalyanasundaram, K. *Coord. Chem. Rev.* **1982**, 46, 159.
- (17) Watanabe, T.; Honda, K. *J. Phys. Chem.* **1982**, 86, 2617.
- (18) Kim, Y. I.; Atherton, S. J.; Brigham, E. S.; Mallouk, T. E. *J. Phys. Chem.* **1993**, 97, 11802.
- (19) Derycke, I.; Vigneron, J. P.; Lambin, Ph.; Lucas, A. A.; Derouane, E. G. *J. Chem. Phys.* **1991**, 94, 4620.
- (20) Amouyal, E.; Zidler, B. *Israel J. Chem.* **1982**, 22, 117.
- (21) (a) Yonemoto, E. H.; Riley, R. L.; Kim, Y. I.; Atherton, S. J.; Schmehl, R. H.; Mallouk, T. E. *J. Am. Chem. Soc.* **1992**, 114, 8081. (b) Cooley, L. F.; Headford, C. E. L.; Elliott, C. M.; Kelley, D. F. *J. Am. Chem. Soc.* **1988**, 110, 6673. (c) Kelly, L. A.; Rodgers, M. A. J. *J. Phys. Chem.* **1995**, 99, 13132.
- (22) Yonemoto, E. H.; Saupe, G. B.; Schmehl, R. H.; Hubig, S. M.; Riley, R. L.; Iverson, B. L.; Mallouk, T. E. *J. Am. Chem. Soc.* **1994**, 116, 4786.
- (23) Kelly, L. A.; Rodgers, M. A. J. *J. Phys. Chem.* **1994**, 98, 6386.
- (24) Bradley, P. G.; Kress, N.; Horneberger, B. A.; Dallinger, R. F.; Woodruff, W. H. *J. Am. Chem. Soc.* **1981**, 103, 7441.
- (25) *Energy Resources Through Photochemistry and Catalysis*; Grätzel, M., Ed.; Academic Press: New York, 1983.
- (26) (a) Sauvage, J.-P.; Collin, J.-P.; Chambron, J.-C.; Guillerez, S.; Coudret, C.; Balzani, V.; Barigelli, F.; De Cola, L.; Flamingini, L. *Chem. Rev.* **1994**, 94, 993. (b) Hoffman, M. Z.; Bolletta, F.; Moggi, L.; Hug, G. L. *J. Phys. Chem. Ref. Data* **1989**, 18, 219.
- (27) Hoffman, M. Z. *J. Phys. Chem.* **1988**, 92, 3458.
- (28) Rodgers, M. A. J.; Becker, J. C. *J. Phys. Chem.* **1980**, 84, 2762.
- (29) (a) Gemborys, H. A.; Shaw, B. R. *J. Electroanal. Chem. Interfacial Electrochem.* **1986**, 208, 95. (b) Li, Z.; Wang, C. M.; Persaud, L.; Mallouk, T. E. *J. Phys. Chem.* **1988**, 92, 2592.
- (30) Li, Z.; Mallouk, T. E. *J. Phys. Chem.* **1987**, 91, 643.
- (31) (a) Gaines, G. L., III; O'Neill, M. P.; Svec, W. A.; Niemczyk, M. P.; Wasiekiwski, M. R. *J. Am. Chem. Soc.* **1991**, 113, 719. (b) Marcus, R. A. *J. Phys. Chem.* **1990**, 94, 4963. (c) Chen, P.; Meyer, T. J. *Inorg. Chem.* **1996**, 35, 5520.
- (32) Jones, W. J., Jr.; Chen, P.; Meyer, T. J. *J. Am. Chem. Soc.* **1992**, 114, 387.
- (33) Hanke, W.; Möller, K. *Zeolites* **1984**, 4, 244.
- (34) Bursner, D.; Steiner, U. F. *Coord. Chem. Rev.* **1994**, 132, 51.
- (35) (a) Sun, H.; Yoshimura, A.; Hoffman, M. Z. *J. Phys. Chem.* **1994**, 98, 5058. (b) Ceulemans, A.; Vanquickenborne, L. G. *J. Am. Chem. Soc.* **1981**, 103, 2238.
- (36) (a) Chen, P.; Duesing, R.; Graff, D. K.; Meyer, T. J. *J. Phys. Chem.* **1991**, 95, 5850. (b) Harriman, A.; Heitz, V.; Ebersole, M.; van Willigen, H. *J. Phys. Chem.* **1994**, 98, 4982. (c) Helms, A.; Heiler, D.; McLendon, G. *J. Am. Chem. Soc.* **1991**, 113, 4325.
- (37) Newton, M. D.; Ohta, K.; Zhong, E. *J. Phys. Chem.* **1991**, 95, 2317.
- (38) Zicovich-Wilson, C. M.; Corma, A.; Viruela, P. *J. Phys. Chem.* **1994**, 98, 10863.
- (39) Larson, S. L.; Cooley, L. F.; Elliott, C. M.; Kelley, D. F. *J. Phys. Chem.* **1992**, 114, 9504.
- (40) Balzani, V.; Scandola, F. In *Energy Resources through Photochemistry and Catalysis*; Grätzel, M., Ed.; Academic: New York, 1983, p 1.
- (41) Yoon, K. B.; Hubig, S. M.; Kochi, J. K. *J. Phys. Chem.* **1994**, 98, 3865.
- (42) Liu, X.; Iu, K.; Thomas, J. K. *J. Phys. Chem.* **1994**, 98, 7877.
- (43) Mercedes, A.; Garcia, H.; Garcia, S.; Marquez, F.; Scaiano, J. C. *J. Phys. Chem. B* **1997**, 101, 3043.